International Journal of Engineering & Technology, 7 (4.25) (2018) 147-153

International Journal of Engineering & Technology

Website: www.sciencepubco.com/index.php/IJET

Research paper

Aerodynamics of a Blended Wing Body Aircraft with Close-Coupled Tail: Computational Fluid Dynamics Simulations of Two Different Tail Sweep Angle Cases

Nur Azan Haiqal Mohamed Shafari, Rizal Effendy Mohd Nasir*, Mohamad Zulfazli Arief Abd Latif, M. Aiman Ahmad, Wirachman Wisnoe, Wahyu Kuntjoro

Aviation Technology Research Group, Flight Technology & Test Centre, Faculty of Mechanical Engineering, University Teknologi MARA, 40450 Shah Alam, Selangor Malaysia
**Corresponding author E-mail: rizal524@salam.uitm.edu.my*

Abstract

This paper presents the aerodynamic performance of Baseline V blended wing-body aircraft via Computational Fluid Dynamic (CFD) simulation. Baseline V has a set of close-coupled tail plane that can change its incidence and tilt angle for pitch and yaw control. Based on previous research, Baseline V has insufficient longitudinal stability in term of pitch moment at zero angle of attack which is negative value at zero tail incidence angles. When tail incidence is set at −10°, the moment coefficient at zero angle of attack is zero thus not sufficient for trim flight with stable pitch moment slope. This leads to the idea of sweeping the tail of the aircraft to increase moment arm. In this paper, two cases are considered which is 0° (case I) and 30° (case II) tail sweep angle in which both cases have tail incidence at −10°. NUMECA suit is used as computational tool for this simulation. The simulated environment consists of half-model Baseline V BWB in domain 20 times the length of the aircraft with body centre plane acts as a mirror. The angle of attack used for this simulation is between -10° to +17° while airspeed is fixed at 15m/s or Mach 0.05. Due to aircraft's small mean chord and low airspeed flight, its Reynold number is low at 1.0 x 10^5 even at its body chord. Therefore, Laminar Navier-Stoke Equation is used for the computational simulation. Lift, drag and pitch moment coefficients with respect to angle of attack for both tail cases are computed from the simulation. The results from the CFD simulation is then compared with wind tunnel experiment results measured at AEROLAB, Universiti Teknologi Malaysia. The result shows that the trends of lift, drag and moment coefficients against angle of attack obtained from CFD simulations are similar to plots obtained from wind tunnel experiment for both tail sweep angle cases. It is found that tail sweep angle case of 30° has slightly less lift but higher drag coefficients compared with 30° tail sweep angle case while its pitch moment coefficient at zero angle of attack has now improved to allow positive trim angle of attack. However, the former has much lower maximum lift-to-drag ratio than the latter.

Keywords: *Aerodynamics, Blended Wing Body, Computational Fluid Dynamic*.

1. Introduction

Blended Wing-Body (BWB) aircraft has the potential to be more efficient than current conventional configuration [1]. Various designs of small BWB UAVs have been studied in past 13 years in Universiti Teknologi Mara and found that not all BWB designs are efficient because aerodynamic efficiency depends on many factors [2]. However, compared to the conventional aircraft with separated fuselage and wing, a Blended Wing-Body aircraft design has proven to be able to generate more lift, less parasitic drag, and improve fuel efficiency to more than 20%. Studies show that, for 800-passenger aircraft, a BWB can offer 15% reduction in take-off weight and 27% reduction in fuel burn per seat mile [3], and significantly reduces noise (environmental friendly) [4] that shows great improvements compared with conventional fuselage-wing aircraft design of today.

Proposed for more than two decades with countless research and study from all over the world, BWB aircraft's proponents are still convincing aircraft manufacturer to mass produce their BWB designs for civil aviation purpose but none has achieved any considerable success other than small scale prototypes. Although BWB aircraft design seems to be a clear solution to the limitation of aerodynamic efficiency of current conventional aircrafts, it still have certain challenges that need to be tackled to ensure safe operation.

A BWB aircraft is a configuration where the wing and fuselage are integrated and blended which almost look like a large flying wing [5] although BWB can have separate stabilizing and control plane such as tail plane and canard fore plane. The fuselage are mostly designed to also generate lift that, compared with conventional aircraft, reduces wetted area for the same weight and planform area of the aircraft. This lifting-body aircraft usually has a wide aerofoil-like body [6]. It is found that this configuration significantly reduces various drag force's types [7][8] such as lift-induced drag, skin friction drag, interference drag, and profile drag, hence significantly improve its lift-to-drag ratio – a measure of aircraft's aerodynamic efficiency. The low wing-body load (lift per planform area) reduces required structural strength and weight thus BWB aircraft is able to reduce maximum take-off weight up to 15% for the same payload capability of the conventional aircraft [8].

One of the unique BWB aircraft designs is VX KittyHawk that is configured with a delta wings to generate enough lift at low speed flight. Delta wings benefit from vortex lift at increased angles of attack, allowing them to achieve higher lift coefficients at higher

Copyright © 2018 Authors. This is an open access article distributed under the Creative Commons Attribution License, which permits unrestricted use, distribution, and reproduction in any medium, provided the original work is properly cited.

angles of attack. However, high angle of attack flight also increases drag force [9].

Other than careful attentions on aerodynamic shapes that influences flight performance [10], control surface configuration and placement on BWB aircrafts are tricky and sometimes seems to be out of norms. It is often found that issues concerning stability and control emerged after one succesful succesful flight [11][12]. For tail-less BWB aircraft, the non-existence of separate horizontal tail behind is a disadvantage in term of longitudinal stability but can still be stabilized and trimmed at particular angle of attack via elevons deflecting up. However, this may cause large trim drag depending on the strength of pitch moment [9].

The multiple coupling of various disciplines which include inertial forces, aerodynamic loads, elastic deformations and flight control system responses on the BWB aircraft affect its performance and stability [4][8][13] that multiple simulations during design process are needed. The shape of many BWB aircrafts can sometimes be challenging to be manufactured easily [7]. Therefore, multidisciplinary optimization (MDO) algorithms has become as important as the design shape of the BWB aircraft itself [14].

In addition, the wetted area and shock strength of a BWB aircraft design need to be balanced in order to minimize drag [3]. Aerodynamic performance and efficiency from less-than-ideal spanwise lift distribution affects lift and induced drag, and also increases drag from the reflex centerbody aerofoil. To lower the drag coefficient, one shall enforce the lift and geometric constraint in the design [7]. A high fidelity method of Euler-based, single-point planform of BWB achieves almost 40% drag reduction at a targeted lift coefficient. Drag can further be reduced by increasing geometric flexibility [14].

Computational simulations or Computational Fluid Dynamics (CFD) has been used by many to investgate, validate or optimize aerodynamics on a BWB aircraft. Navier-Stoke CFD in both inverted design and direct solution shall be considered for final geometry [3]. By RANS solver, the conservation law needs to be controlled by a cell-centred finite volume approach [10]. In comparisons with the conventional tail and wing (CTW) aircrafts [15], the BWBs are optimized using grids with $1.5x10^9$ nodes, and the CTWs use grids with $6.3x10^6$ nodes. It was described in Reist and Zingg [16] that those nodes will accurately predict the correct friction/pressure drag ratio and thus capture the drag trade-offs associated with changes in wing area.

The aerodynamics of inviscid optimizer (ASO) shall also be considered for cruise condition calculation [17]. Only then the goal towards the multi-disciplinary optimization (MSO) shall be achieved. Both Euler node solver and RANS node grids have the same grid resolution on the surface, i.e. the same number and distribution of nodes in the chord-wise, span-wise and wall-adjacent normal directions. In design approach, it is suggested that planform optimization design to be the dominant step followed by wing section inverse design as supplementary step [18].

The result of aerodynamic parameters such as lift, drag and moment coefficients obtained from CFD simulation is often verified by results from wind tunnel. A study is conducted at Langley Full Scale Tunnel [11] where the experiment involves testings of BWB aircraft aerodynamics at low speed; tumble, rotary, baseline large angle force oscillation, free flight and ground effect. It is necessary to validate the data obtained from computational calculation with the actual wind tunnel in order to simulate the aircraft with actual condition of airflows and drags.

In 2016, a team of researchers from Universiti Teknologi Mara proposes a novel planform of BWB aircraft resembling flying-wing but with extended lifting body incorporating a close-coupled horizontal tail that not only can have its elevator change its incidence for pitch control but can also tilt its tail for yaw control. The reason of the new design is to enable yawing control without having a rudder on vertical tail[19]. It has been tested in UiTM's LST-1 wind tunnel and in AEROLAB UTM with varying angle of attack at actual flight speed of 15 m/s (54 km/h) for five elevator angle cases at zero tilt angle and varying sideslip angle for four tilt angle cases at one fixed elevator angle. The result shows that the aircraft's highest lift-to-drag ratio is 32.0 and at 3.0 degree angle of attack. It is also found that Baseline-V is statically stable in pitch and yaw but has no clear indication in terms of roll stability**.**

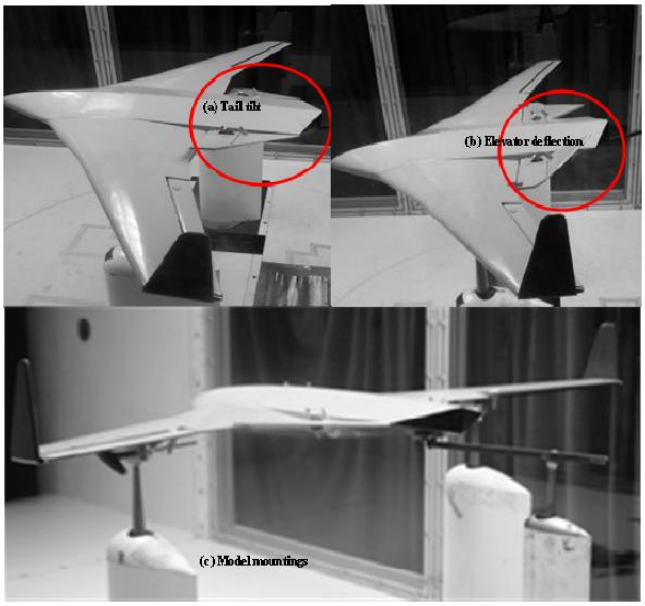

Fig 1: Baseline-V BWB with a close-coupled tail [19]

The design is a results of years of experience in evolution of BWB design studies since 2005. Baseline V is based on lessons learned in Baseline-I which is a tail-less, cranked planform BWB [20] and Baseline II [21] which is a radical change from its predessessor for having smooth wing-body blend. Using Inverse-Twist method, Baseline II can achieve excellent L/D of 25.0 [22] but with extremely strong nose-down moment (too stable) that a small, medium-aspect ratio control canard has to be added at the nose of its body for positive trim angle of attack [23], however, its maximum lift-to-drag ratio reduces to just mere 19.0. In the meantime, Baseline II BWB with a broad chord, short span canard (low aspect ratio) is analyzed to produce maximum lift-to-drag ratio of 10.0 [24]. Better aerodynamic performance shall be achieved if the aircraft obtains a relaxed CG location.

2. Problem Statement and Hypothesis

Baseline V has insufficient longitudinal stability in term of pitch moment at zero angle of attack which is negative value at zero tail incidence angles. When tail incidence is set at −10°, the moment coefficient at zero angle of attack is zero thus not sufficient for trim flight with stable pitch moment slope. This leads to the idea of sweeping the tail of the aircraft to increase moment arm. Without rebuilding the whole BWB configuration, one could control aerodynamics centre, or neutral point, towards aft by increasing the sweep angle which alters the static margin. Sweeping the angle of tail can be the factor to improve its stability by increasing moment at zero angle of attack to positive value while maintaining negative pitch moment-angle of attack slope without too much penalty on lift-to-drag ratio. Therefore, this study focuses on sweeping the angle of tail by referring it as case I and case II for or 0° and 30° tail leading edge sweep angle, respectively.

3. Methodology

Table 1 below shows the simulated conditions, tools and model equations:

Table 1: simulated conditions, tools and model equations

Parameter	Scope of research
Model Used	BWB Baseline V UAV Half Body ,UiTM
Angle of Attack	-10° to 17°
Sweep Tail	0° and 30° only
Speed	15m/s
Mach number	0.05
CAD Software	CATIA and Solidwork
CFD Software	NUMECA
Flow Model	Laminar Navier-Stoke Equation

The work begins by drafting Baseline V BWB CAD model in CATIA as shown in Table 2. The CAD model must be converted into parasolid (.x_t) file. By opening product file in CATIA and then saved as Initial Graphics Exchange Specifications (.igs or IGES), it enables the drawing to be opened using Solidwork software. In Solidwork, the product drawing is converted into parasolid (.x_t) file to be used in NUMECA. . The simulated environment consists of half-model Baseline V BWB in domain 20 times the length of the aircraft with body centre plane acts as a mirror.

For the result to be no longer dependent on the number of cells, grid sensitivity study needs to be performed. CFD parameter validation will be performed after the grid independent is achieved. This is shown in the Figures 2 and 3 for both case I and case II respectively at -10° angle of attack. Three cases of number of cell are tested – 0.5, 1.5 and 3.0 million and the team has agreed that the number of cells above 1.5 million is good enough produce satisfactory, consistent computation results. There are three processes in CFD simulation – pre-processing, processing and post-processing. The pre-processing stage uses Hexpress as meshing tools to determine whether the mesh quality is acceptable. Processing is executed by FineOpen in NUMECA where the computational simulation takes place. The parameter of the simulation is set up to be the same as the wind tunnel conditions in order to get the same exact condition. CFView is used as visualization tool.

Table 2: Drawing for Baseline V for Case I and Case II

Tail sweep angle	Side/Plan View
0° Case I	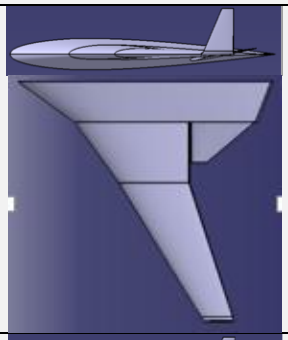
30° Case II	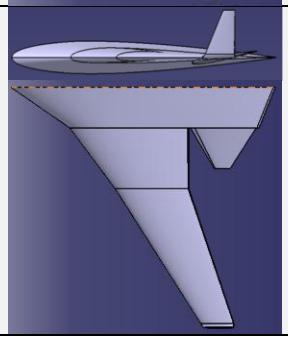

4. Results

Figure 4 shows the lift coefficient, C_L between CFD simulation and wind tunnel experiment versus angle of attack, α for Case I and Figure 5 for Case II. For both cases, the plots' trendlines are assumed to be in cubic order within -20° < □□ < +20° range. Comparisons between CFD simulation and wind tunnel experiment data in these two figures validates the accuracy of Laminar Navier-Stokes model implemented in the simulation especially within the so-called 'linear lift region' which is between -10° < □□ < +10° range. Maximum lift coefficients for both cases are around 0.79-0.80 at angles of attack between 17° to 20°. Cubic C_L versus □□ trendline equations shown in Figures 4 and 5 in both cases have extremely small third and second-order constants that one can simply estimate the linear lift curve slope, dC_L/d□ and zero angle of attack lift, C_{Lo} directly. The slope is higher for Case I at 0.066 per degree than Case 2 at 0.056 per degree while C_{Lo} for the former is 0.012 – higher than -0.023 recorded for the latter's C_{Lo}. However, these two C_{Lo} is too insignificantly small on the plot with respect to full range of C_L values that it is assumed that $C_{Lo} \approx 0.0$.

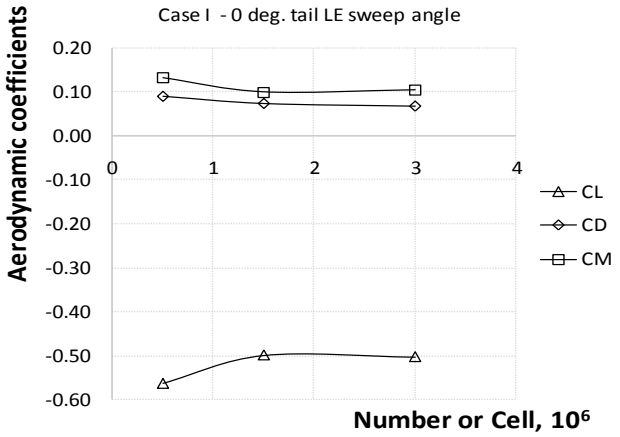

Fig 2: Grid Independent Study for Swept Angle 0° Tail

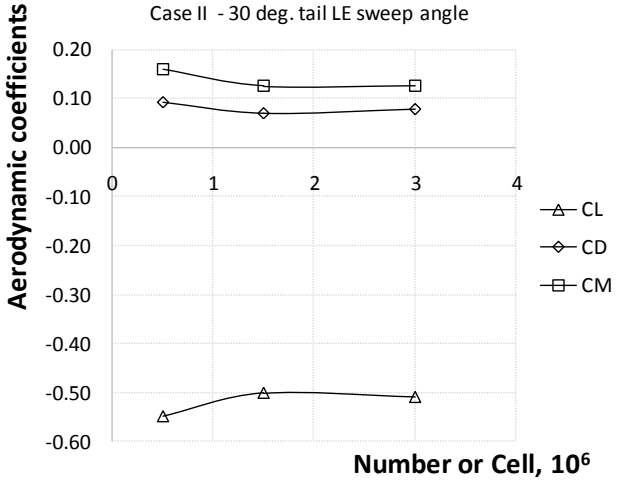

Fig 3: Grid Independent Study for Swept Angle 30° Tail

Figure 6 and Figure 7 show plots of drag coefficient against angle of attack for both Case I and Case II respectively. For Case I, minimum drag coefficient occur sat α = 0° for CFD simulation and wind tunnel experiment. This shows a good agreement between the two method of investigation. Trendlines are set to be parabolic in shape just like many actual aircrafts. From trendline equations, one can find some important parameters of drag such as induced drag factor K and drag at zero lift coefficient C_{Do}. Since C_L at zero angle of attack is very small (near zero), the drag at zero lift C_{Do} can be read directly from C_D versus a plot by looking at the last number in the parabolic trendline equations in Figures 6 and 7. In this study it is found that C_{Do} for 30° tail sweep angle is higher at 0.0242 than 0° tail sweep angle cases at 0.0105. The reason as to why drag coefficient increases as tail sweep angle increases is perhaps due to the tail sweep angle itself. At zero tail

sweep angle (Case I), the tail is very close to the trailing edge of the wing that it almost "hide" itself from incoming airflow where as in Case II the tail sweep angle at 30° causes airflow behind the wing to directly impact the tail plane.

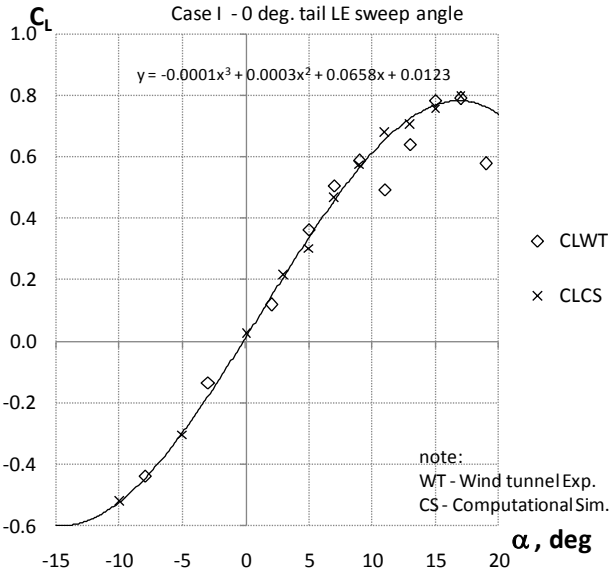

Fig 4: Lift coefficient against angle of attack for Case I

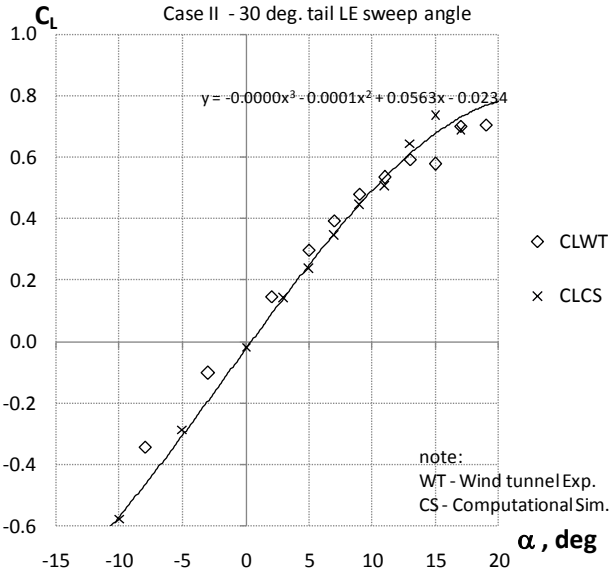

Fig 5: Lift coefficient against angle of attack for Case II

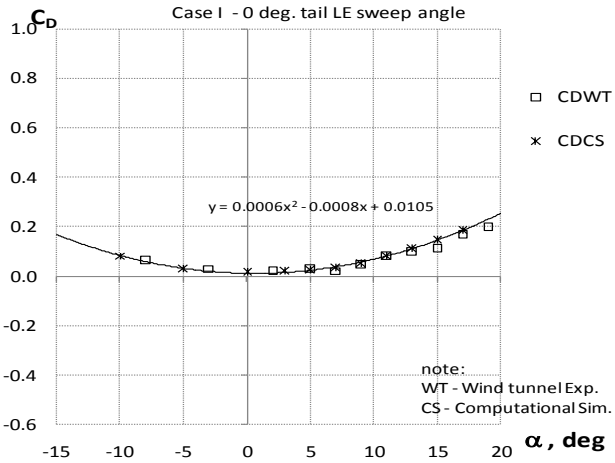

Fig 6: Drag coefficient against angle of attack for Case I

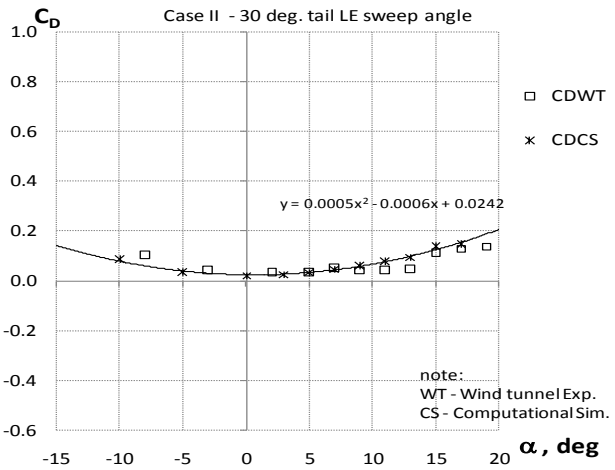

Fig 7: Drag coefficient against angle of attack for Case II

The curves of pitch moment coefficient, C_M versus angle of attack, α are presented in Figure 8 and Figure 9 for Case I and Case II respectively. Similar in approach to lift coefficient plots, cubic equation regression is used to produce trendlines for pitch moment versus angle of attack plots. From both aforementioned figures, Case I's trendline seems to be curvier than Case II's in which the latter looks almost linear. Again, just like lift coefficient trendlines, the constants for third and second order part of the trendline equations can simply being ignored for angles of attack within 'linear lift region'. Within this region, the CM versus a trendline looks linear.

Two important stability parameters need to be highlighted here is the slope of the plot and pitch moment where Case I has $dC_M/d\alpha$ = -0.022 and $C_{Ma=0}$ = -0.0054. This is lower than $dC_M/d\alpha$ = -0.014 and $C_{Ma=0}$ = 0.024. Alternatively, since C_{Lo} for both cases is approximately zero then, the change of pitch moment with respect to the change of lift $dC_M/dC_L = dC_M/d\alpha \times d\alpha/dC_L$ or negative of static margin, $-K_n$ is -0.3 and -0.25 for Case I and Case II respectively. This shows that static margin of the BWB aircraft is 30% mean chord and 25% mean chord for Case I and Case II, respectively. In the meantime, zero-lift pitch moment C_{Mo} is now equals to $C_{Ma=0}$. For both cases, the negative slope and positive value of pitch moment at zero lift indicating that the aircraft is statically longitudinally stable. Trim angle of attack for Case II is 1.5°.

The curves of L/D versus angle of attack, α are shown in Figure 10 and figure 11 for case I and case II respectively. For both cases, the maximum L/D in CFD simulation are less than the experimental L/D value. Maximum L/D for Case 1 is 14.0 while for Case 2, the maximum L/D is 7.0 only. For both cases, the angle of attack at maximum L/D is at 6.0 -7.0°. Since trim angle of attack for Case II is 1.7° then its trim L/D is around 3.0 only! Take note that the tail incidence is already set at -10°. In order to trim to optimal angle of attack where L/D is the highest, the one and only possible way now is to increase the magnitude of tail incidence which will further increase the drag hence decrease L/D_{max} further down.

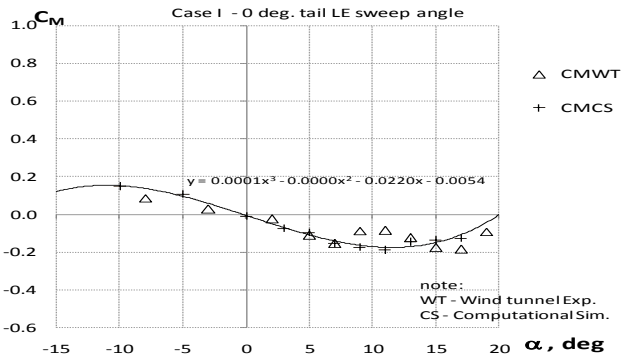

Fig 8: Pitch moment coefficient against angle of attack for Case I

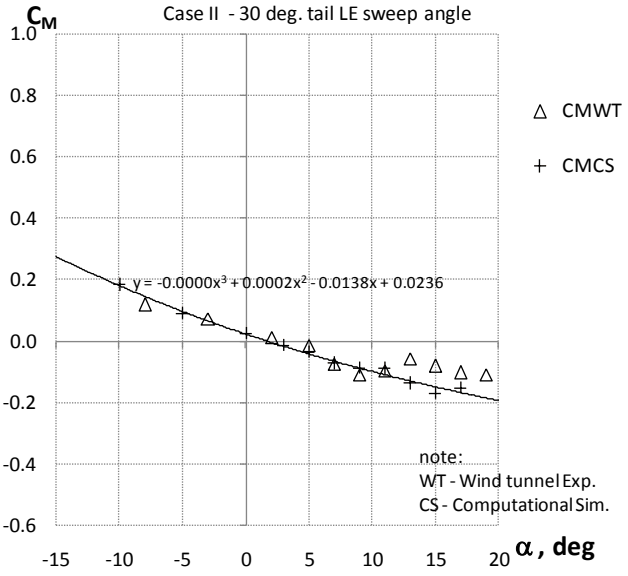

Fig 9: Pitch moment coefficient against angle of attack for Case II

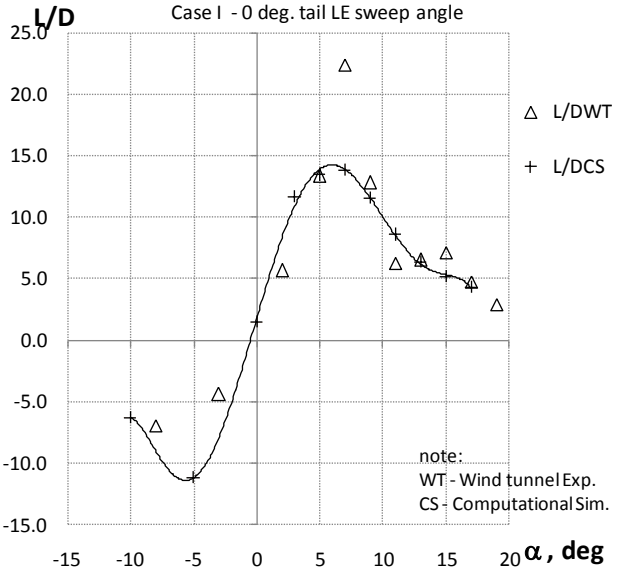

Fig 10: Lift-to-Drag ratio against angle of attack for Case I

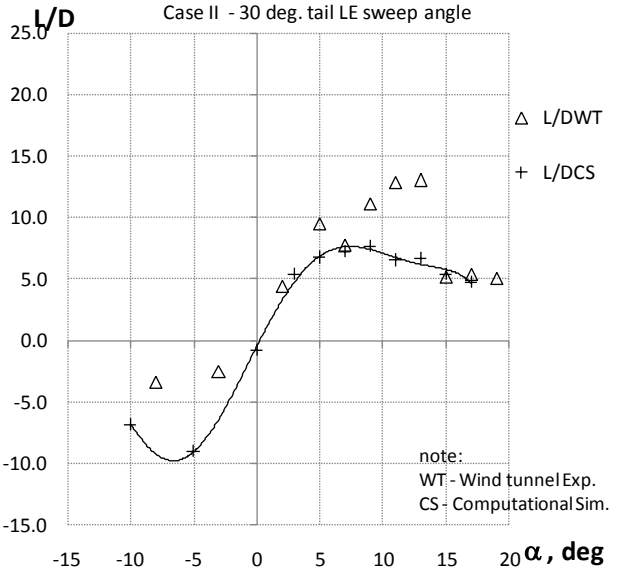

Fig 11: Lift-to-Drag ratio against angle of attack for Case II

Figure 12 shows velocity profile while Figure 14 shows pressure contour of the aircraft during its highest lift to drag ratio. From both figure, we can see the aircraft still generate lift force as the velocity on the top is higher than the bottom region which causes the pressure at the top region is lower than the bottom region. Meanwhile at +9° angle of attack, the L/D begin to drop which shown in Figure 13 and figure 15 whereby the velocity starts to move slower than before and the pressure became higher than before at top region from the intensity shown.

Figure 16 shows velocity profile and Figure 18 shows pressure contour of the aircraft during its highest lift –to-drag ratio. From both figure, we can see the intensity of velocity is higher at above region and the pressure is lower compared to the bottom region. At +11° angle of attack, the intensity shows the same pattern as case I which is the velocity become less and the pressure become more at the top region. Figure 17 and 19 show the velocity profile and pressure contour respectively. Since the velocity decreases at angle of attack +11°, a blue-black background is used to make the velocity streamline colour visible for figure 17.

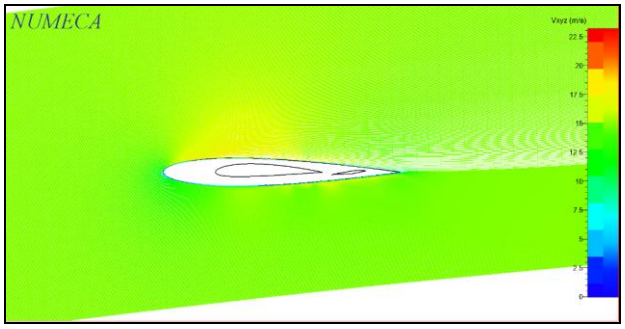

Fig 12: Velocity profile at 7° angle of attack, Case

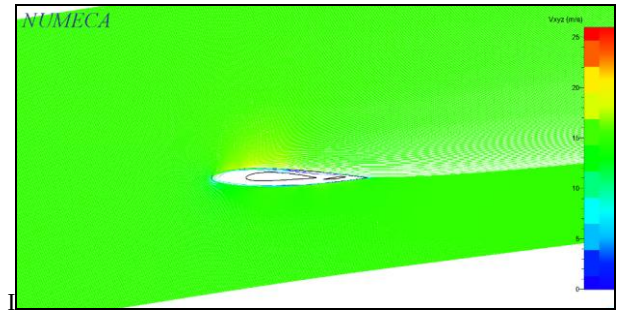

Fig 13: Velocity profile at 9° angle of attack, Case

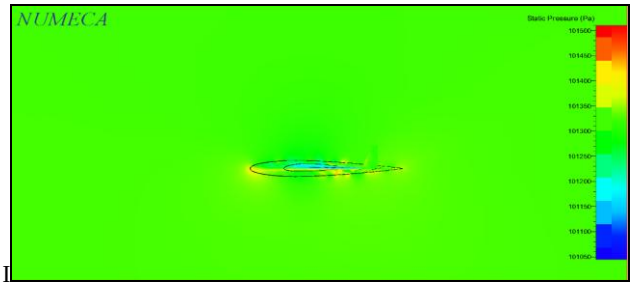

Fig 14: Pressure Contour at 7° angle of attack, Case

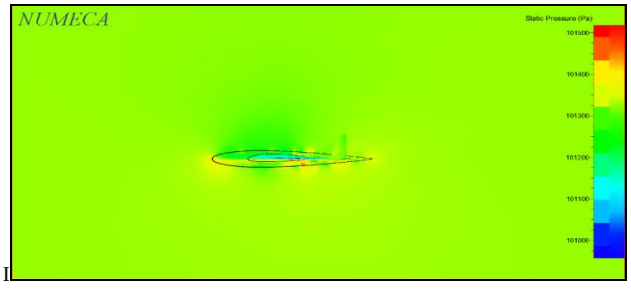

Fig 14: Pressure Contour at 7° angle of attack, Case

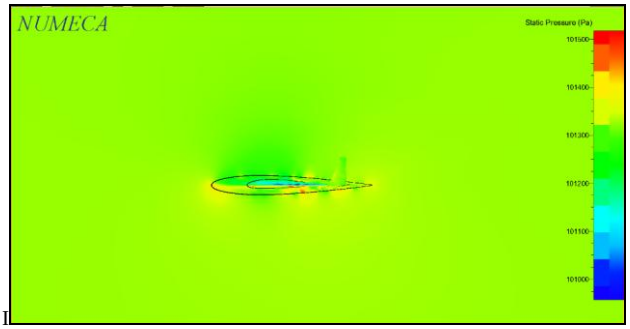

Fig 15: Pressure Contour at 9° angle of attack, Case

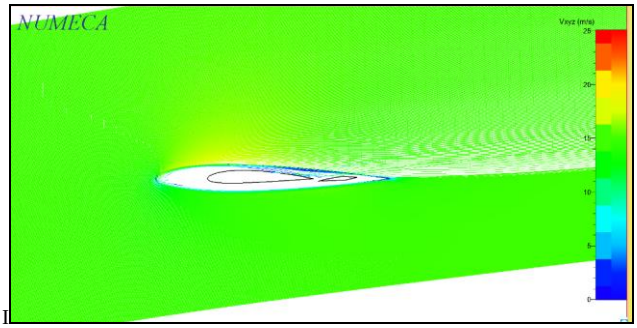

Fig 16: Velocity profile at 9° angle of attack, Case II

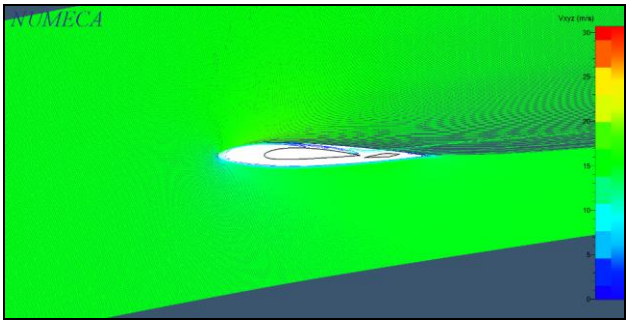

Fig 17: Velocity profile at 11° angle of attack, Case II

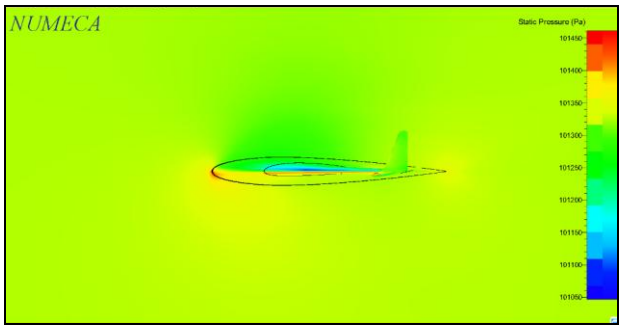

Fig 18: Pressure Contour at 9° angle of attack, Case II

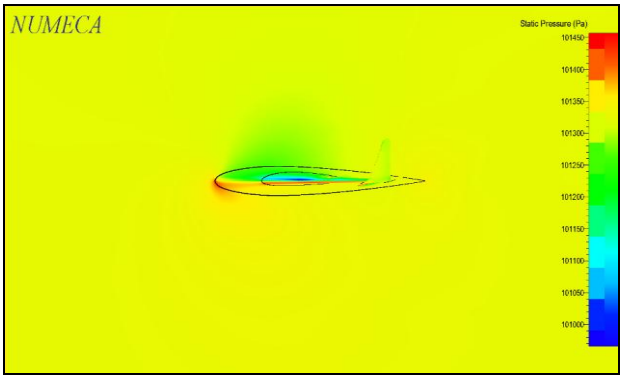

Fig 19: Pressure Contour at 11° angle of attack, Case II

5. Concluding Remarks

Plots from CFD simulations presented here show similar trends for lift coefficient, drag coefficient and moment coefficients for both cases compared with wind tunnel experiment plots. Tail sweep of 30° has lower value of lift coefficient for a given angle of attack due to lower lift curve slope, higher drag coefficient at zero lift, and slightly relaxed stability (less steep pitch moment slope). However, maximum lift-to-drag ratio has decreased tremendously from around 14.0 to only 7.0 if switching from 0° tail sweep angle to 30° tail sweep angle setup. Although trim angle of attack has increased to 1.7°, it is still insufficient because the most efficient angle of attack of this aircraft is around 6.0-7.0°. In short, the results of this study are summarized in Table 3.

Table 3: Summary of results

Parameters	Case I; 0° tail sweep	Case II; 30° tail sweep
$dC_L/d\square$	+0.066/°	+0.056/°
C_{Lo}	+0.01 ≈ 0.0	-0.02 ≈ 0.0
C_{Lmax}	0.79	0.80
$\square_{CLmax}$	17.0°	20.0°
C_{Do}	0.010	0.024
K’	-0.012	-0.011
$K = 1/(\square eAR)$	0.14	0.16
L/D_{max}	14.0	7.0
$\square_{L/Dmax}$	6.0°	7.0°
$dC_M/d\square$	-0.022/°	-0.014/°
$C_{M\square=0} \approx C_{Mo}$	-0.005 ≈ 0.0	0.024
$\square_{trim}$	0.0°	1.7°
$dC_M/ dC_L = -K_n$	-0.30	-0.25

If one were to maintain tail sweep angle of 30° without resorting to increase the magnitude of tail incidence to trim to L/D_{max} then one of the solution is to move the centre of gravity backwards so that static margin become only 5%. However, with L/D_{max} of only 7.0 which is worse than conventional aircraft then perhaps the original design with 0° tail sweep angle would make more sense because of its high L/D and with advance electronic control available at cheap price, longitudinal stability and control will not become a big issue then.

Acknowledgment

Authors would like to express deepest gratitude to The Faculty of Mechanical Engineering Universiti Teknologi MARA for sponsoring publication of this research and research facility support. We would also like to express our gratitude to staffs of AEROLAB Universiti Teknologi Malaysia. Our thanks are also dedicated to the Research Management Institute for GIP Research Grant (600-IRMI/MYRA 5/3/GIP (037/2017)).

References

[1] Z. Lyu and J. R. R. a. R. A. Martins, “Aerodynamic Design Optimization Studies of a Blended-Wing-Body Aircraft,” *J. Aircr.*, vol. 51, no. 5, pp. 1–14, Sep. 2014.

[2] R. E. M. Nasir, F. Mohamed, R. Ramly, A. M. I. Mamat, W. Wisnoe, and W. Kuntjoro, “Flight Performance of Various Blended Wing- Body Small UAV Designs,” *J. Teknol.*, vol. 5, pp. 103–109, 2015.

[3] R. H. Liebeck, “Design of the Blended Wing Body Subsonic Transport,” *J. Aircr.*, vol. 41, no. 1, pp. 10–25, 2004.

[4] P. Okonkwo and H. Smith, “Review of evolving trends in blended wing body aircraft design,” *Progress in Aerospace Sciences*, vol. 82, Pergamon, pp. 1–23, 01-Apr-2015.

[5] T. Ikeda and C. Bil, “Aerodynamic performance of a blended-wing-body configuration aircraft,” *Congr. Int. Counc.of Aeronaut. Sc.*, pp. 1–10, 2006.

[6] P. Dehpanah and A. Nejat, “The aerodynamic design evaluation of a blended wing-body configuration,” *Aerosp. Sci. Technol.*, vol. 43, pp. 96–110, Jun. 2015.

[7] Z. Lyu and J. R. R. A. Martins, “Aerodynamic Shape Optimization

of a BlendedWing-Body Aircraft," in *51st AIAA Aerospace Sciences Meeting including the New Horizons Forum and Aerospace Exposition*, 2013, no. June, pp. 1–17.

[8] N. Qin, A. Vavalle, A. Le Moigne, M. Laban, K. Hackett, and P. Weinerfelt, "Aerodynamic considerations of blended wing body aircraft," *Progress in Aerospace Sciences*, vol. 40, no. 6. Pergamon, pp. 321–343, 01-Aug-2004.

[9] C. M. Boozer, M. J. Van Tooren, and A. Elham, "Multidisciplinary Aerodynamic Shape Optimization of a Composite Blended Wing Body Aircraft," *58th AIAA/ASCE/AHS/ASC Struct. Struct. Dyn. Mater. Conf.*, 2017.

[10] N. Qin, A. Vavalle, and A. Le Moigne, "Spanwise Lift Distribution for Blended Wing Body Aircraft.," *J. Aircr.*, vol. 42, no. 2, pp. 356–365, 2005.

[11] Dan D. Vicroy, "Blended-Wing-Body Low-Speed Flight Dynamics :," pp. 1–10, 2009.

[12] J.-Y. T. Ammar Sami, Clément Legros, "Conceptual design, performance and stability analysis of a 200 passengers Blended Wing Body aircraft," *Aerosp. Sci. Technol.*, Sep. 2017.

[13] P. P. C. Okonkwo, "Conceptual Design Methodology for Blended Wing Body Aircraft," *Sch. Aerospace, Transp. Manuf.*, vol. Ph.D., 2016.

[14] N. B. Kuntawala, J. E. Hicken, and D. W. Zingg, "Preliminary Aerodynamic Shape Optimization Of A Blended-W ing-Body Aircraft Conguration," *AIAA-2011-642*, January, 2011.

[15] T. A. Reist and D. W. Zinggy, "Aerodynamic design of blended wing-body and lifting-fuselage aircraft," in *34th AIAA Applied Aerodynamics Conference, 2016*, 2016.

[16] T. Reist and D. W. Zingg, "Aerodynamically Optimal Regional Aircraft Concepts: Conventional and Blended-Wing-Body Designs," *52nd Aerosp. Sci. Meet.*, no. January, pp. 1–13, 2014.

[17] N. B. Kuntawala *et al.*, "Aerodynamic Shape Optimization of a Blended-wing-body Aircraft Configuration," *Aerosp. Sci. Technol.*, vol. 29, no. 1, p. 111, Apr. 2011.

[18] L. I. Peifeng *et al.*, "Aerodynamic design methodology for blended wing body transport," *Chinese J. Aeronaut.*, vol. 25, no. 4, pp. 508–516, 2012.

[19] R. E. M. Nasir, N. S. C. Mazlan, Z. M. Ali, W. Wisnoe, and W. Kuntjoro, "A blended wing body airplane with a close-coupled, tilting tail," *IOP Conf. Ser. Mater. Sci. Eng.*, vol. 152, p. 012021, 2016.

[20] W. Wisnoe, R. E. Mohd Nasir, W. Kuntjoro, and A. Mohd, "Wind Tunnel Experiments and CFD Analysis of Blended Wing Body (BWB) Unmanned Aerial Vehicle (UAV) at Mach 0.1 and Mach 0.3," *13th Int. Conf. Aerosp. Sci. Aviat. Tech.*, 2009.

[21] Wisnoe, W., Kuntjoro, W., Mohamad, F., Mohd Nasir, R. E., Reduan, N. F., & Ali, Z. (2010). Experimental results analysis for UiTM BWB baseline-I and baseline-II UAV running at 0.1 mach number. *International Journal of Mechanics*, *4*(2), 23-32.

[22] Nasir, R. E. M., Kuntjoro, W. , Wisnoe, W., Ali, A., Reduan, N.F., Mohamad, F. and Suboh, S. 2010. Preliminary Design of "Baseline-II" Blended Wing-Body (BWB) Unmanned Aerial Vehicle (UAV): Achieving Higher Aerodynamic Efficiency Through Planform Redesign and Low-Fidelity Inverse Twist Method. Proceedings of 3rd Engineering Conference on Advancement in Mechanical and Manufacturing for Sustainable Environment (EnCon2010), Kuching, Sarawak, Malaysia. April 14-16, 2010.

[23] R. E. M. Nasir, W. Kuntjoro, and W. Wisnoe, "Aerodynamic, Stability and Flying Quality Evaluation on a Small Blended Wing-body Aircraft with Canard Foreplanes," *Procedia Technol.*, vol. 15, pp. 783–791, Jan. 2014.

[24] Z. M. Ali, W. Kuntjoro, and W. Wisnoe, "The Effect of Canard to the Aerodynamic Behavior of Blended Wing Body Aircraft," *Appl. Mech. Mater.*, vol. 225, no. 5, pp. 38–42, 2012.